

LOSS ANALYSIS OF BACK-CONTACT BACK-JUNCTION THIN-FILM MONOCRYSTALLINE SILICON SOLAR CELLS

F. Haase¹, S. Eideloth¹, R. Horbelt^{1,*}, K. Bothe¹, E. Garralaga Rojas¹, and R. Brendel^{1,2}

¹Institute for Solar Energy Research Hamelin (ISFH), Am Ohrberg 1, 31860 Emmerthal, Germany

²Institute of Solid State Physics, Leibniz Universität Hannover, Appelstr. 2, 30167 Hannover, Germany

*Now with University of Konstanz, Jacob-Burckhardt-Str. 29, 78464 Konstanz, Germany

ABSTRACT

We investigate the power losses in back-contact back-junction monocrystalline thin-film silicon solar cells. The cells are made from epitaxial layers grown on and separated from porous Si (PSI process). We combine two-dimensional finite element modeling with a resistance network simulation. The simulated and measured current-voltage characteristics agree. Free energy loss analysis reveals that the main limiting loss mechanism of the best cell with 13.5 % efficiency is the high saturation current density at the metal-silicon interface of 5×10^4 fA cm⁻², causing 2.5 % absolute efficiency loss.

INTRODUCTION

We already reported a process for back-contact back-junction (BC BJ) monocrystalline thin-film silicon solar cells using the PSI process [1]. A porous layer etched into the surface of a substrate wafer, served as predetermined breaking point for the lift-off of an epitaxial grown layer. The epitaxial layer had a thickness of 30 μ m and an area of 79.2 cm². The cell was processed from this epitaxial layer and had a planar front surface, an efficiency of 13.5 %, and a fill factor of 74 % [1]. The short circuit current density was 28.7 mA cm⁻² and the open circuit voltage was 633 mV [1]. In the previous report we did not analyze the relative significance of various loss mechanisms. This analysis is the purpose of this contribution. Standard techniques are quantum efficiency analysis [2], electroluminescence imaging [3], light beam induced current mapping (LBIC), and J-V-curve measurements. However, the interpretation of these is not straight forward for BC BJ cells. Simulations of the BC BJ cells are required to understand the measurements. Probably, the most widespread simulation tool is PC1D programmed by Clugston and Basore [4]. Since this is a one dimensional simulation tool and our cell is not laterally homogeneous, it can hardly model our BC BJ solar cell.

Instead, we use a two-dimensional conductive boundary (CoBo) model as recently described [5] for solar cell simulations. Highly doped regions at the surface like emitters and back surface fields (BSFs) are treated as one-dimensional conductive boundaries. The conductivity and saturation current density characterize the boundaries. We determine these input data for the conductive boundary simulation by measuring test samples processed with the same processes as the solar cells. The series resistance of the aluminum fingers and the contact resistance are not considered by the CoBo simulations. We perform a resis-

tance network simulation using LTSpice [6] to account for this effect. The combination of CoBo and LTSpice simulations is capable of modeling the measured J-V-curves.

Free energy loss analysis [7] serves for identification of the efficiency limiting factors of solar cell performance. This analysis calculates the power losses per area of all recombination and transport losses in our cell at the maximum power point so that we can compare all these losses directly.

CELL GEOMETRY

The back-contact back-junction cell has an interdigitated finger structure. Figure 1 shows a schematic cross section of half of a unit cell. A stack of amorphous silicon/silicon nitride passivates the front and the back surface. The rear surface of the unit cell consists of a base and an emitter finger. Both fingers have local contacts to the aluminum.



Figure 1 Schematic of the cross section of half of a unit cell. The drawing is not to scale.

Figure 2a shows a schematic of the top-view with the full-length local contact openings that are visible prior to the aluminum deposition. In a second type of samples we decrease the contact area by a factor of three by having gaps in the line contact openings, shown in Figure 2b. Figure 2c shows the definition of the unit cells for the resistance network simulation.

EXPERIMENTAL

Table 1 lists the saturation current densities of the different surfaces as determined by measuring test samples. The samples are prepared with the same processes as the cells. However the geometries were selected to allow an easy evaluation. The calculations of the saturation current densities are based on lifetime measurements with infrared lifetime mapping. A detailed description of the determination of these saturation current densities will be published elsewhere [8].

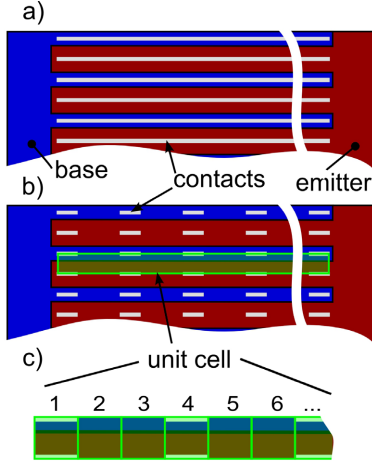


Figure 2 Schematic top view of the local contacts. Figure 2a shows the full line contact openings. Figure 2b shows the broken line contact openings. Figure 2c shows the unit cells of the resistance network simulation

Table 1 Saturation current densities of cell surfaces

Region	Front surface	Passiv. emitter	Met. emitter	Passiv. base	Met. base
J_0 [fAcm ⁻²]	5	90	4000	5	50000

In this paper, we investigate four groups of BC BJ thin-film silicon solar cells. Group A and C have full line contact openings, whereas group B and D have broken line contacts, as shown in Figure 2. Group A and B have a 20 times higher base doping than group C and D. All the resistances listed in Table 2 are measured on test samples. The transfer length method serves for contact resistance measurements [9], whereas four-point probe measurements serve for determination of the sheet resistance of the base and of the emitter. The aluminium finger and the emitter finger width are smaller than the width of the unit cells. Therefore, the sheet resistance has to be weighted with the fraction of finger width w_{finger} to unit cell width $w_{unitcell}$:

$$R_{finger} = \frac{\rho_{finger}}{d_{finger}} \times \frac{w_{finger}}{w_{unitcell}} \quad (1)$$

All parameters of the four groups A to D are listed in Table 2.

SIMULATIONS

We combine a two-dimensional half unit cell simulated using the CoBo model [5] with a series resistance network simulation using LTSpice [6] in order to reproduce the measured J-V-characteristics. The CoBo software performs a pure electrical simulation and optical effects are not taken into account. Therefore, we use a generation profile that we model with the software SUNRAYS [10] as input data for our cell simulation. The two-dimensional

CoBo model generates a characteristic illuminated current-voltage-curve. It does not consider the contact resistances of the silicon-metal interface, the series resistances of aluminum fingers and series resistances of the base and of the emitter fingers in the third dimension.

Table 2 Parameters of the four cell groups

Group	A	B	C	D
Full line contacts	Yes	No	Yes	No
Base doping [cm ⁻³]	3×10^{16}	3×10^{16}	1.5×10^{15}	1.5×10^{15}
Cell area [cm ²]	79.2	79.2	5.2	5.2
Bulk lifetime τ_{bulk} [μs]	4	10	2	2
$R_{Al\ base\ finger}$ [Ω sq ⁻¹]	0.016	0.016	0.016	0.016
$R_{base\ contacts}$ [Ω cm ²]	0.01	0.01 or 1×10^5	0.1	0.1 or 1×10^5
R_{base} [Ω sq ⁻¹]	170	170	3000	3000
$R_{emitter}$ [Ω sq ⁻¹]	150	150	150	150
$R_{emitter\ contacts}$ [Ω cm ²]	0.001	0.001 or 1×10^5	0.001	0.001 or 1×10^5
$R_{Al\ emitter\ finger}$ [Ω sq ⁻¹]	0.0025	0.0025	0.0025	0.0025

We perform a series resistance network simulation using LTSpice in order to include the effect of the resistance losses. The busbar of the solar cell is wide and thus has a low series resistance. Therefore, it does not influence the network simulation and we simulate a single finger that is divided in unit cells as shown in Figure 2c. Figure 3 shows schematically the network of resistances. The photodiodes exhibit the CoBo-simulated illuminated J-V-characteristics.

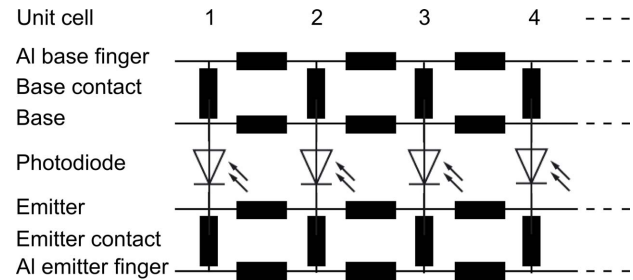


Figure 3 Series resistance network of a single finger consisting of unit cells 1, 2, 3, ...

FREE ENERGY LOSS ANALYSIS OF THE UNIT CELL

Table 3 shows the power density losses of the unit cells of group A and B obtained from the free energy loss analysis [7] of the finite element simulations. Group A has full line contacts along the finger so that every unit cell of the resistance network has a contact opening. Group B has gaps in the line contact openings where the cell is passivated and the unit cell has no contact opening. In these unit cells we use a high contact resistance of 1×10^5 Ω cm².

The unit cells with contacts are dominated by base contact recombination. Shockley-Read-Hall (SRH) recombination is only limiting the performance in the passivated unit cell of group B. The groups with BSF are simulations of hypothetical cells for the determination of the efficiency potential. An implementation of a BSF with a saturation current density of 500 fA cm^{-2} in contact group B would decrease the losses to 35 W m^{-2} . An additional texture would increase the free energy generation and would result in a 27 W m^{-2} higher extracted power density.

Table 3 Power density generation, sum of losses and main losses in $[\text{W m}^{-2}]$ of the unit cells of the four cell groups simulated with the CoBo model.

Unit cell group:	Contact A	Contact B	Passiv. B	Contact B BSF	Contact B BSF texture
Generation	191	192	195	194	226
Sum of losses	52	46	28	35	40
Base contact recombination	25	26	0	10	12
SRH recombination in base	13	6	12	10	11
Bulk transport of electrons	11	11	10	10	11
Others	3	3	6	5	6
Extracted free energy	139	146	167	159	186

COMPARISON OF SIMULATIONS WITH EXPERIMENTS

Figure 4 shows the simulated and measured J-V-curves of all groups. Every group presents three J-V-curves: The measured illuminated curve, the measured $J_{SC}-V_{OC}$ curve, and the output of the combined simulation of unit cell and series resistance network.

The measured illuminated curves and the curves of combined unit cell and network simulation are in agreement in all cases. The measured $J_{SC}-V_{OC}$ curves show high pseudo-fill factors (FF) of 76 % to 80 % compared to the FF in the illuminated J-V-curves of 45 % to 74 %. The difference of both curves shows the losses due to the resistances mentioned in Table 2.

The FF -limiting resistances are the base contact resistance and the base resistance. Groups A and B have a factor of 20 higher base doping and therefore a lower base resistance and a lower base contact resistance when compared to groups C and D. This results in a higher FF . Groups A and C have full line contacts whereas group B and D have gaps in the contact lines. The current has a shorter path to the contact lines and therefore the base resistance has less influence in group A and C. This effect results in a higher FF for group A and C. Combining the first and the second effect, group A has the highest FF

whereas group D has the lowest FF with an FF -loss of 32 % absolute compared to the pseudo- FF .

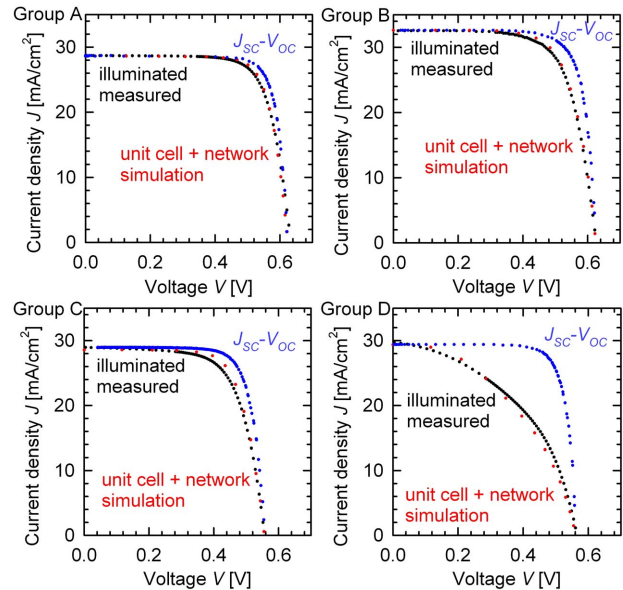


Figure 4 IV-curves of the different cell groups.

CONCLUSIONS AND OUTLOOK

We present a detailed loss analysis of BC BJ monocrystalline thin-film silicon solar cells. The saturation current densities that we measured on test samples and the modeled generation profile are input data to J-V-curve simulations using the two-dimensional CoBo model. In combination with series resistance network simulation, the simulated current-voltage characteristics are in agreement with experimental measurements. Free energy loss analysis identifies the base contact with a saturation current density of $5 \times 10^4 \text{ fA cm}^{-2}$ as the main efficiency limiting mechanism in our current cell design. It causes 2.6 % absolute efficiency loss. Local contact resistances of $0.1 \Omega \text{ cm}^2$ in combination with a high base resistance lead to fill factor reductions of 32 % absolute. Our simulations show that introducing a BSF could decrease the power loss to 35 W m^{-2} and the efficiencies would increase to 15.4 %. The use of a front surface texture could increase the generated free energy to 226 W m^{-2} and hence the efficiency to 18 %.

ACKNOWLEDGEMENTS

The authors thank Dörthe Schiewe and Renate Winter for their valuable help with sample processing.

REFERENCES

- [1] F. Haase et al., "Back contact monocrystalline thin-film silicon solar cells from the porous silicon process", *34th IEEE PVSC*, 2009, pp. 244-246.

- [2] B. Fischer, PhD thesis, "Loss analysis of crystalline silicon solar cells using photoconductance and quantum efficiency measurements", University of Konstanz, *Cuvillier: Göttingen*, 2003.
- [3] K. Bothe et al., "Electroluminescence imaging as an in-line characterisation tool for solar cell production", *21st EPVSEC*, 2006, pp. 597-600.
- [4] D. A. Clugston, and P. A. Basore, "PC1D Version 5: 32-bit solar cell modelling on personal computers", *26th IEEE PVSC*, 1997, pp. 207-210.
- [5] R. Brendel, "Modeling solar cells with the dopant-diffused layers treated as conductive boundaries", *Progress in Photovoltaics: Research and Applications*, n/a. doi: 10.1002/pip.954
- [6] LTspice IV, Linear Technology, <http://www.linear.com/designtools/software/> (accessed on Feb. 16, 2011)
- [7] R. Brendel et al., "Theory of analyzing free energy losses in solar cells", *18th NREL Workshop on Crystalline Silicon Solar Cells & Modules*, 2008, pp. 113-116.
- [8] F. Haase et al., *Journal of Applied Physics*, submitted for publication.
- [9] G. K. Reeves, and H. B. Harrison, "Obtaining the specific contact resistance from transmission line model measurements", *IEEE Electron Dev. Lett.* **3**, 111 (1982).
- [10] R. Brendel, "SUNRAYS: A versatile ray tracing program for the photovoltaic community", *12th EPVSEC*, 1994, pp. 1339-1342.